ISSN (Print) 1226-1750
ISSN (Online) 2233-6656
Journal of Magnetics 25(2), 157-163 (2020) https://doi.org/10.4283/JMAG.2020.25.2.157

Effect of Gradient Linearity and Static Magnetic Field Homogeneity on Diffusion Weighted Image: A Phantom Study

Ho-Beom Lee[1,2], Yong-Soo Han[1,3], and Sung-Min Kim[1]*

[1]*Department of Medical Device Industry Dongguk University, Seoul 04620, Republic of Korea*
[2]*Asan Medical Center, 88, Olympic-ro, Songpa-gu, Seoul 05505, Republic of Korea*
[3]*Department of Radiological Science, Hanlym Polytechnic University, Chuncheon 24210, Republic of Korea*

(Received 22 January 2020, Received in final form 11 May 2020, Accepted 11 May 2020)

In this study, we assessed image quality and geometric accuracy as a function of the gradient physical linearity used for diffusion-weighted imaging (DWI) on both conventional-bore and wide-bore scanners. The signal to noise ratio (SNR) was calculated using b = 1000 DWI images for all acquisitions. To evaluate geometric accuracy, the diameter of a phantom on an image slice was measured in four directions. In comparison with the enhanced gradient mode, the default and maximum gradient modes showed higher SNRs with both bore sizes. There were significant differences in SNR among the various gradient modes of the two bore sizes. The geometric accuracy evaluations showed no statistically significant differences in the measured lengths among the various gradient modes and both bore sizes. The wide bore using default and maximum gradient mode showed higher SNR than the conventional bore, and comparable geometric accuracy.

Keywords : MR-Imaging, gradient physical linearity, static magnetic homogeneity

1. Introduction

With technical developments in MRI (magnetic resonance imaging, MRI), gradient strength and slew rate have increased with developments in coil design, optimized cooling, power supply, and stronger gradient amplifiers. Gradient strength affects spatial resolution and imaging scan time, as well as the gradient switching rates (dB/dt) for simultaneously switching the encoding gradients in all three axes, and these parameters are critical for MRI. The linearity of the gradient coil describes the deviation from an ideal linear 'steepness' of the magnetic field. A low physical linearity of the gradient coil will result in image distortions and in a smaller maximum field of view (FOV). The distortions can be corrected by software means with a distortion correction algorithm applied on the reconstructed images, but this comes at the expense of lower spatial resolution in the periphery of the FOV, due to an interpolation involved in the 'expansion' of collapsed voxels. However, a lower linearity will increase the efficiency of the gradient coil with respect to max. amplitude and max. slew rate [1, 2].

In particular, rapid scanning sequences such as diffusion-weighted echo-planar imaging (EPI) require high gradient strengths, high slew rates, and rapid gradient switching rates, as the encoding improves in an approximately linear relationship with the gradient strength and the square root of the slew rate [2]. Furthermore, the diffusion-weighted EPI sequence uses pulsed gradients, and the faster the imaging sequence, the greater the gradient switching rates required.

The recent development of wide-bore (70 cm) high-field MRI scanners provides improved comfort and less stress to larger patients and those with claustrophobia [3, 4]. However, to maintain homogeneity of the magnetic field, they have a relatively lower gradient strength than conventional-bore scanners (60 cm). In addition, previous studies reported that wide-bore scanners inevitably have worse geometric accuracy than conventional-bore scanners, as the magnetic field inhomogeneity and gradient field nonlinearity increase with increasing distance from the iso-center [5, 6]. However, to date, there is no report evaluating whether the various gradient modes that change the strength of gradient switching in diffusion-weighted imaging (DWI) effect image quality and geometric accuracy differently between conventional and wide-bore scanners.

*Corresponding author: Tel: +82-2-3010-4325
Fax: +82-2-3010-6788, e-mail: sungmin2009@gmail.com

Therefore, the purpose of this study was to investigate image quality and geometric accuracy as a function of gradient mode in DWI, making comparisons between conventional-bore and wide-bore scanners.

2. Materials and Methods

2.1. Phantom experiment study

As in a previous study [7], an MR phantom accredited by the American College of Radiology (ACR; JM, Specialty Parts, San Diego, CA, USA) was used for the phantom measurements. The internal measurements of the ACR phantom are a length of 148 mm and diameter of 190 mm. The phantom was filled with a solution of nickel chloride and sodium chloride (10 mM $NiCl_2$ and 75 mM NaCl [8]), and was carefully aligned and positioned in the center of each head coil with the spatial orientation defined according to its nose and chin marks. The phantom was then scanned at room temperature (21.0 °C) to nullify the quantitative measurements showing temperature dependence. The phantoms were kept in the same MRI room with a temperature logger, and using consistent coil and phantom support arrangements, with the identical sequence version and parameters each week.

2.2. Image acquisition

All images were acquired on a clinical 60 cm conventional-bore 3-Tesla MR scanner with an 80 mT/m maximum gradient strength and a 200 T/m/s maximum slew rate (Ingenia CX; Philips Healthcare, Eindhoven, the Netherlands), or on a clinical 70 cm wide-bore 3-Tesla MR scanner with a 45 mT/m maximum gradient strength and a 200 T/m/s maximum slew rate (Ingenia; Philips Healthcare, Eindhoven, the Netherlands). A 32-channel head coil (Philips Healthcare) was used for both scanners. DWI sequences with two b-values (0 and 1000 s/mm^2) were acquired in the axial plane. The DWI parameters included were as follows: field of view, 250 × 250 mm; pixel size, 1.95 × 1.95 mm; acquisition matrix, 128 × 128; flip angle, 90°; time of repetition (TR), shortest; time of echo (TE), shortest; slice thickness, 5 mm; slice gap, 5 mm; number of slices, 11; sensitivity encoding, 2.5 (P reduction, AP); number of acquisitions, 2; half scan factor, 0.811; and phase-encoding direction, anterior to posterior. Slice thickness and slice gap were set according to the ACR phantom test guidelines [8]. A detailed summary of the DWI parameters of all the gradient modes is presented in Table 1. A dual-type gradient system was used in this study. The peak amplitude (G) is the strength of the gradient system in mT/m. For a given gradient coil, the gradient strength is directly proportional to the current according to the following equation:

$$G = \eta I \quad (1)$$

where G = gradient amplitude, I = the current in the coil generated by the gradient amplifier, and η = the coil sensitivity2, which describes the gradient strength achieved per ampere of current.

The slew rate is often referred to as the speed of the gradient system. It describes how fast a certain gradient amplitude can be switched on and off, starting from 0 mT/m. It is related to the rise time it takes to achieve a certain gradient amplitude and is defined by the following equation:

$$SR = G / Trise \quad (2)$$

where SR = slew rate, Trise = rise time, and G_{max} and SR_{max} represent the gradient performance.

The two gradient amplifiers for each gradient axis can be switched in parallel or in serial mode: the parallel mode results in high current (= high amplitude) but low voltage (= low slew rate), while the serial mode results in high voltage (= high slew rate) but low current (= low amplitude). The consequence of this switching is that the imaging sequence can only use (i) a high amplitude setting (maximum mode), (ii) a high slew rate setting (enhanced mode), or (iii) a moderate amplitude and slew rate setting (default mode).

Table 1. Summary of single-shot diffusion-weighted imaging parameters as a function of gradient mode for conventional and wide-bore scanners.

Conventional bore (60 cm)			
Gradient mode	Default	Maximum	Enhanced
TR (ms)	3000	3000	3000
TE (ms)	69	66	54
Bandwidth (Hz)	24.3	29.6	27.1
dB/dt (T/s)	62.7	95.6	62.7
Scan time (s)	103	103	103
Wide bore (70 cm)			
Gradient mode	Default	Maximum	Enhanced
TR (ms)	3000	3000	3000
TE (ms)	77	74	60
Bandwidth (Hz)	24.3	29.4	25.7
dB/dt (T/s)	59.3	118.6	53.4
Scan time (s)	103	103	103

2.3. Image analysis

The location of the ACR phantom slice 7, where the phantom was uniform, was used for the signal to noise ratio (SNR) analysis. The SNR is calculated at the high b-

value b = 1000, respectively. The SNR values of the DWI were calculated using the National Electrical Manufacturers Association subtraction method 1 [9] according to the following equation:

$$\mathrm{SNR} = \frac{S}{\sigma/\sqrt{2}}, \tag{3}$$

$$\sigma = \left[\frac{\Sigma_{i=1}^{n}\Sigma_{j}^{m_i}(R(i,j)-\bar{R})^2}{\Sigma_{i=1}^{n}(m_i)-1}\right]^{1/2} \tag{4}$$

where S is the mean signal value of two images and σ is the standard deviation of the subtracted image. S and σ were derived from the same region of interest (ROI) applied to the two images and the subtracted image. Where $\bar{R}$ is the average of an ROI, $R(i, j)$ is an individual pixel within the ROI, and n and m are the pixel numbers in the row and column directions. The $\sqrt{2}$ factor arises because noise with propagation of error is derived from the difference image [9, 10]. Image analysis was performed with ImageJ (ImageJ v. 1.45; National Institutes of Health, Bethesda, MD, USA). Apparent diffusion coefficient (ADC) values were calculated from the EPI-DWI according to the following equations [11]:

$$b = \gamma^2 G^2 \delta^2 \left(\Delta - \frac{\delta}{3}\right) \tag{5}$$

$$\mathrm{ADC} = -\frac{\mathrm{In}\left[\frac{S(b_2)}{S(b_1)}\right]}{(b_2 - b_1)}, \tag{6}$$

where G, γ, Δ, and δ are the gradient pulse magnitude, gyromagnetic ratio, time interval, and duration, the inter-pulse delay and the pulse duration define the diffusion time. respectively. S_1 and S_2 are the signal intensities acquired at the low b-value b_1 and the high b-value b_2, respectively. For the evaluation of geometric accuracy, the diameter of the phantom on image slice 5 was measured in four directions: top to bottom, left to right, and along both diagonals (Fig. 1).

2.4. Statistical Analysis

The Kolmogorov–Smirnov test was used to determine whether dependent variables were normally distributed. On the basis of the results of the Kolmogorov–Smirnov test, the SNR of the different b-value DWI images and the ADC maps obtained with the various gradient modes and both scanners were compared using either analysis of variance (ANOVA) or a Kruskal–Wallis test. When statistically significant differences were demonstrated, post-hoc tests were performed using the Tukey–Kramer method. Statistical analyses were performed using IBM SPSS Statistics for Windows/Macintosh, v. 21.0 (IBM Corp., Armonk, NY, USA). For all statistical analyses, a two-sided level of $P < 0.05$ was considered statistically significant. The coefficient of variation (CV) was used to assess the precision of repeated geometric accuracy and ADC value measurements as a function of the gradient mode of both scanners. The CV of five repeated measurements was calculated by dividing the standard deviation by the mean value [11].

3. Results

The SNR and ADC values for the various gradient modes of both scanners are presented in Table 2. The SNR values of the wide-bore scanner were higher than those of the conventional-bore scanner, irrespective of the gradient mode. Contrary to the SNR, the ADC values of

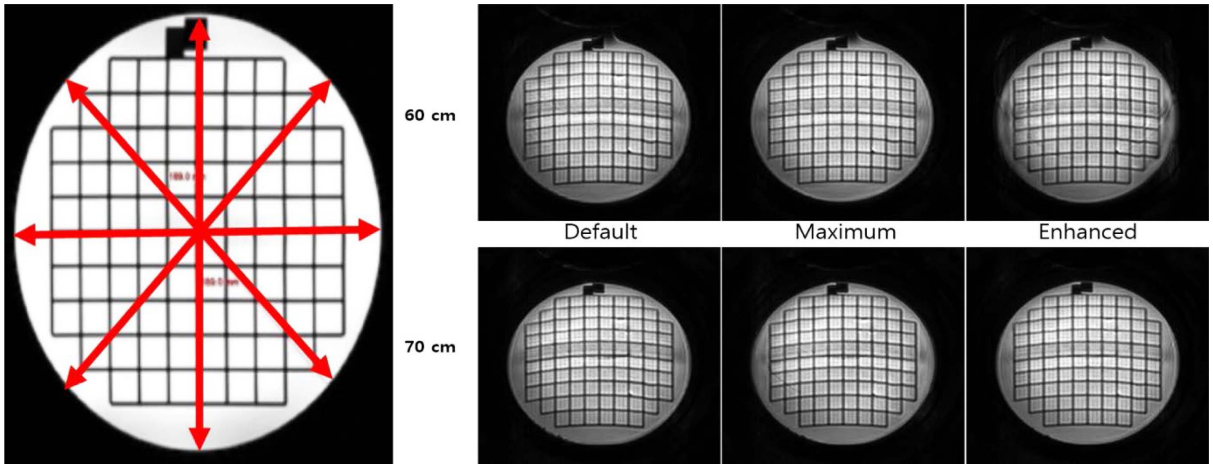

Fig. 1. (Color online) Images used to assess geometric accuracy. The diameter of the phantom image on slice 5 was measured in four directions on images acquired for each of the gradient modes and both scanner bore sizes.

Table 2. SNR and ADC values according to the various gradient modes and scanner bore size.

	Conventional bore (60 cm)		Wide bore (70 cm)	
Mode	SNR	ADC	SNR	ADC
Default	85.05 ± 7.03*†	2.231 ± 0.003*†	105.44 ± 10.48*†	2.174 ± 0.001*†
Maximum	84.11 ± 7.33*†	2.226 ± 0.001*†	107.09 ± 11.35*†	2.162 ± 0.001*†
Enhanced	65.12 ± 4.07*†	2.231 ± 0.003*†	86.68 ± 8.42*†	2.162 ± 0.002*†

When statistically significant differences were demonstrated by post-hoc tests using the Tukey–Kramer method (Tukey corrected p-value < 0.05), the symbols * and † were used to indicate p-values between gradient modes (*), and between bore sizes and gradient modes (†). SNR = signal to noise ratio, ADC = apparent diffusion coefficient.

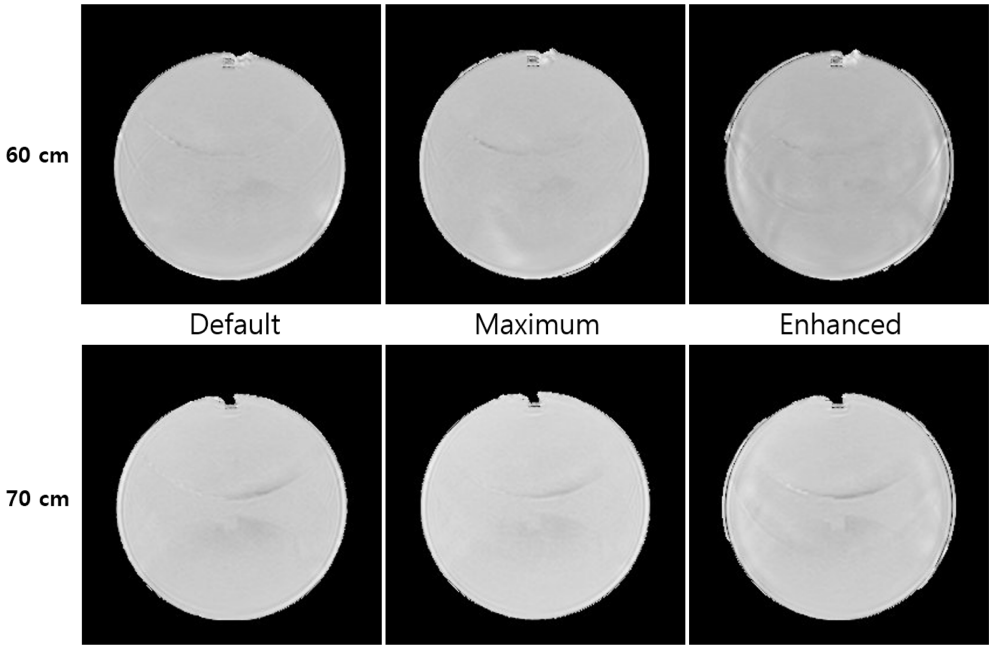

Fig. 2. Apparent diffusion coefficient (ADC) images acquired at various gradient modes and both scanner bore sizes.

the wide-bore scanner were lower than those of the conventional-bore scanner.

ADC value calculated from the various gradient modes and for both bore sizes are presented in Fig. 2. More image noise was observed in the enhanced gradient mode than in the default and maximum gradient modes, with this being the case for both bore sizes. There were significant differences in SNR and ADC among the various gradient modes for the two bore sizes ($p < 0.05$; ANOVA). However, post-hoc tests using the Tukey–Kramer method showed no significant differences within specific group comparisons (Fig. 3; $p > 0.05$). Table 3 shows the results of the geometric accuracy measurements and the CVs calculated for the various gradient modes for both bores. There were no statistically significant differences in the measured lengths between the different gradient modes and the two bore sizes ($p > 0.05$). The CV of ADC values were within 0.26 %, which represents nearly identical geometric accuracy, irrespective of the gradient mode and bore size.

4. Discussion

In the current study, we assessed the SNR, ADC values, and geometric accuracy of DWI acquired using different gradient modes on standard and wide-bore scanners. We found that the various gradient modes resulted in different SNR values for both bores, and that the SNR values of the wide-bore scanner were higher than those of the conventional-bore scanner. In comparison with the enhanced gradient mode, the default and maximum gradient modes showed higher SNR values for both bore sizes. In particular, the wide-bore scanner using the default and maximum gradient modes showed higher SNR than the conventional-bore scanner. However, our findings are not consistent with previous results that showed the signal intensity of a wide-bore scanner to be lower than that of a conventional-bore scanner [12]. The difference may be

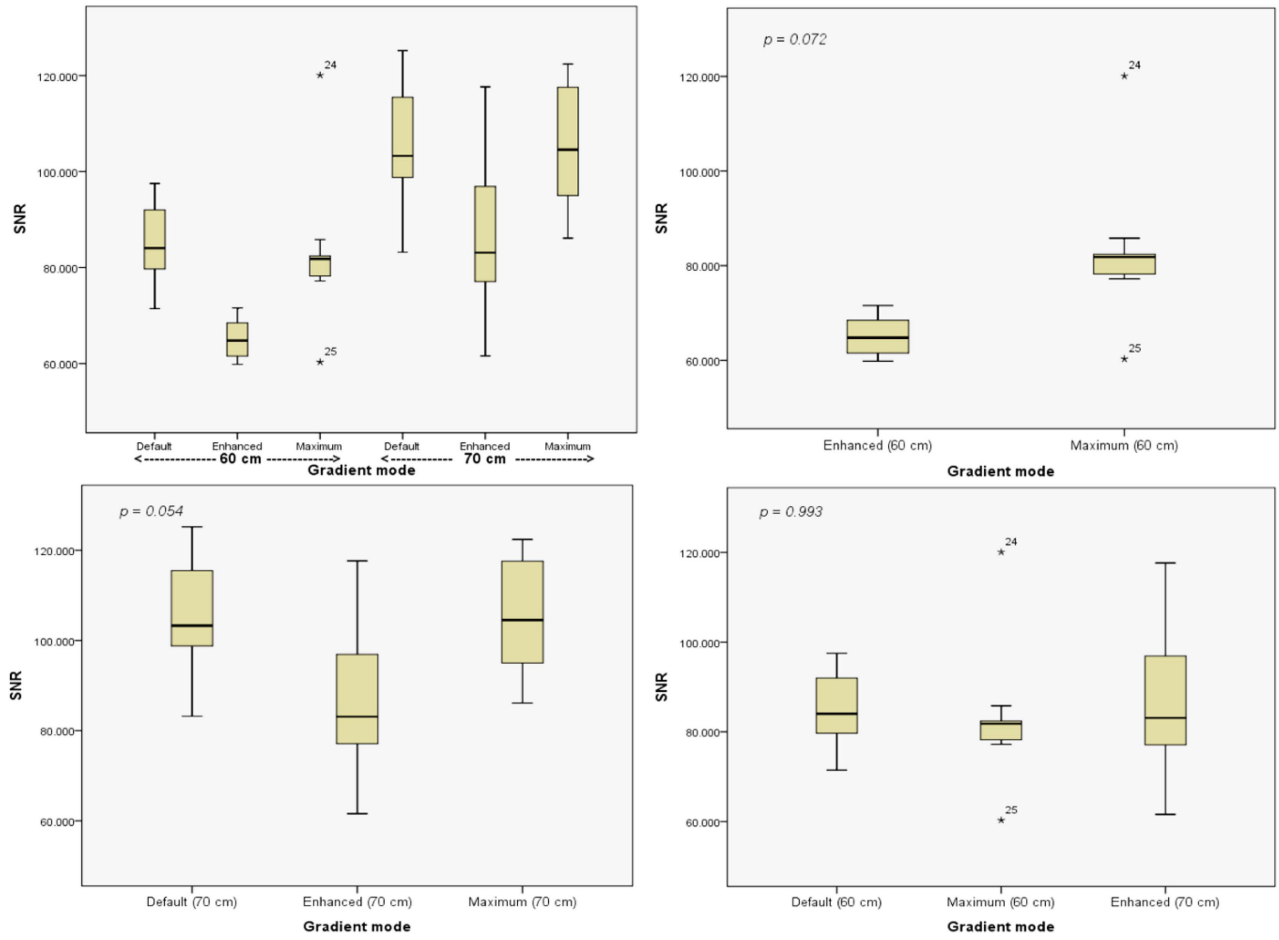

Fig. 3. (Color online) Box-plot graph showing the distribution of the signal to noise ratio (SNR) as a function of the gradient mode for both bore sizes. *Outliers indicate values more than 1.5 times the upper quartile.

Table 3. Geometric accuracy and coefficients of variation (CVs) according to the various gradient modes and scanner bore size.

Bore	Direction	Measurement	Default	Maximum	Enhanced
60 cm	TB	Length (mm)	189.23 ± 0.17	189.26 ± 0.18	189.27 ± 0.31
		CV (%)	0.09	0.09	0.16
	LR	Length (mm)	189.13 ± 0.04	188.83 ± 0.24	188.73 ± 0.16
		CV (%)	0.02	0.13	0.09
	RD	Length (mm)	188.61 ± 0.35	188.43 ± 0.21	188.46 ± 0.22
		CV (%)	0.18	0.11	0.11
	LD	Length (mm)	189.13 ± 0.04	189.06 ± 0.28	189.23 ± 0.23
		CV (%)	0.02	0.15	0.12
70 cm	TB	Length (mm)	189.46 ± 0.11	189.06 ± 0.31	189.26 ± 0.11
		CV (%)	0.06	0.16	0.06
	LR	Length (mm)	189.43 ± 0.35	188.96 ± 0.32	189.26 ± 0.11
		CV (%)	0.18	0.17	0.06
	RD	Length (mm)	188.63 ± 0.49	188.23 ± 0.32	188.36 ± 0.15
		CV (%)	0.26	0.17	0.08
	LD	Length (mm)	188.96 ± 0.41	189.26 ± 0.49	189.03 ± 0.32
		CV (%)	0.21	0.26	0.17

TB = top to bottom, LR = left to right, RD = right diagonal, LD = left diagonal. Length values are expressed as mean ± standard deviation. There were no significant differences in geometric accuracy (all p-values > 0.05).

explained by differences in the acquisition sequences, phantom size, and fields of view, which may have affected image quality.

In terms of geometric accuracy, some studies demonstrated that wide-bore scanners inevitably showed greater geometric distortion than conventional-bore scanners [5, 6]. However, we did not find such a pattern, with our results showing that the various gradient modes showed no significant differences in geometric accuracy between the conventional and wide-bore scanner. This discrepancy may result from the fact that the inhomogeneity and gradient field nonlinearity increase with increasing distance from the iso-center. In addition, in our study, the distance from the iso-center to the analyzed image slices was relatively shorter than in the previous studies cited. Previous research reported that in order to obtain all required measurements for an image after a single excitation pulse with an EPI sequence, the opposite polarity readout gradient is needed; the minimum readout time is determined by the maximum gradient slew rate and amplitude [13]. A longer readout time due to T2* decay results in increased image blurring and distortion. In addition, improvements in gradient amplitude and slew rate will increase acoustic noise and the likelihood of peripheral nerve stimulation, both of which can cause patient discomfort [14-16]. With respect to gradient performance, most studies only state the maximum amplitude of the gradient system and the maximum slew rate. The two key characteristics of the gradient system, the amplitude and slew rate, are often written in the simplified form 'gradient amplitude max / slew rate max'. The gradient slew rate is especially important for fast sequences such as fast gradient echo, true fast imaging with steady-state free precession, and EPI. Single-shot EPI especially depends on the maximum gradient mode [17]. Thus, the choice of gradient mode in EPI-DWI is important to ensure high image quality and geometric accuracy without distortion.

There are some limitations to our study. First, we used only the ACR phantom, which is designed for quality assurance and does not represent different organs, tissues, or lesions such as those due to acute stroke or glioma in real humans. Second, even though we used the shortest TE value and the optimal bandwidth for each gradient mode and scanner bore, the TEs and bandwidths still varied owing to mechanical constraints between the scanners, and these variations could have affected image quality. Lastly, our experiment was designed using only 3-T MRI scanners from one vender. Therefore, further study to demonstrate the influence of a variety of scanner types and magnetic field strengths on image quality is warranted. Nevertheless, our research is meaningful because it is the first experiment evaluating various gradient modes, and comparing image quality and geometric accuracy between two scanners of different bore sizes.

5. Conclusion

The gradient mode influenced the SNR of EPI-DWI on both conventional and wide-bore scanners, although geometric accuracy was maintained. With regard to SNR, both default and maximum gradient modes were superior to the enhanced gradient mode for both bore sizes. Overall, the SNR values from wide-bore scanners tended to be higher than those from conventional-bore scanners, regardless of the gradient mode used.

References

[1] K. Setsompop, R. Kimmlingen, E. Eberlein, T. Witzel, J. Cohen-Adad, J. A. McNab, and S. F. Cauley, Neuroimage **80**, 220 (2013).
[2] M. Weiger, J. Overweg, M. B. Rösler, R. Froidevaux, F. Hennel, B. J. Wilm, and M. Borgo, Magn. Reson. Med. **79**, 3256 (2018).
[3] G. Koch, J. Garnon, G. Tsoumakidou, F. Edalat, J. Caudrelier, R. L. Cazzato, and A. Gangi, J Vasc. Interv. Radiol. **29**, 285 (2018).
[4] J. Stattaus, S. Maderwald, H. A. Baba, G. Gerken, J. Barkhausen, M. Forsting, and M. E. Ladd, Eur. Radiol. **18**, 2865 (2008).
[5] G. P. Liney, S. C. Owen, A. K. E. Beaumont, V. R. Lazar, D. J. Manton, and A. W. Beavis, Br J. Radiol. **86**, 1027 (2013).
[6] H. Nakazawa, M. Komori, Y. Shibamoto, Y. Takikawa, Y. Mori, and T. Tsugawa, J. Med. Imaging Radiat. Oncol. **58**, 595 (2014).
[7] J. S Jang, Y. S. Han, and M. A. Jeong, J. Magn. **24**, 217 (2019).
[8] Z. J. Wang, Y. Seo, J. M. Chia, and N. K. Rollins, Med. Phys. **38**, 4415 (2011).
[9] F. L. Goerner and G. D. Clarke, Med. Phys. **38**, 5049 (2011).
[10] M. J. Firbank, A. Coulthard, R. M. Harrison, and E. D. Williams, Phys. Med. Biol. **44**, 261 (1999).
[11] T. Yoshida, A. Urikura, K. Shirata, Y. Nakaya, S. Terashima, and Y. Hosokawa, Br J. Radiol. **89**, 1065 (2016).
[12] H. B. Lee, J. S. Jang, Y. S. Han, and S. M. Kim, J. Magn. **24**, 471 (2019).
[13] D. L. Parker, K. C. Goodrich, J. R. Hadley, S. E. Kim, S. M. Moon, B. A. Chronik, and F. Schmitt, Concepts Magn. Reson. Part B Magn. Reson. Eng. **35**, 89 (2009).
[14] J. Abart, K. Eberhardt, H. Fischer, W. Huk, E. Richter, T. Storch, and E. Zeitler, J. Comput. Assist. Tomogr. **21**, 532 (1997).

[15] K. F. King and D. J. Schaefer, Magn. Reson. Imaging Clin. N Am. **6**, 731 (1998).
[16] B. Zhang, Y. F. Yen, B. A. Chronik, G. C. McKinnon, D. J. Schaefer, and B. K. Rutt, Magn. Reson. Med. **50**, 50 (2003).
[17] S. S. Hidalgo-Tobon, Concepts in Magnetic Resonance Part A **36**, 223 (2010).